

2D Mixed Convection Viscous Incompressible Flows with Velocity-Vorticity Variables

Alfredo Nicolás¹ and Blanca Bermúdez²

Abstract: Mixed convection viscous incompressible fluid flows, under a gravitational system, in rectangular cavities are reported using the unsteady Boussinesq approximation in velocity-vorticity variables. The results are obtained using a numerical method based on a fixed point iterative process to solve the nonlinear elliptic system that results after time discretization; the iterative process leads to the solution of uncoupled, well-conditioned, symmetric linear elliptic problems for which efficient solvers exist regardless of the space discretization. Results with different aspect ratios A up to Grashof numbers $Gr = 100000$ and Reynolds numbers $Re = 1000$ for the lid driven cavity problem are reported. The validation of the results is given through mesh size and time-step independence studies.

Keywords: velocity-vorticity formulation, mixed convection flows, aspect ratio, Reynolds and Grashof numbers, fixed point iterative process

1 Introduction

Mixed convection viscous incompressible fluid flows, under a gravitational system, in rectangular cavities using the unsteady Boussinesq approximation in velocity-vorticity variables are presented. They are obtained with a numerical procedure based on a fixed point iterative process to solve the nonlinear elliptic system that results once a convenient second order time discretization is made; the iterative process leads to the solution of uncoupled, well-conditioned, symmetric linear elliptic problems for which efficient solvers exist regardless of the space discretization. For the lid driven cavity problem, results with different aspect ratios A ($A =$ ratio of the height to the width) are reported up to Grashof numbers $Gr = 100000$ and Reynolds numbers $Re = 1000$; the lid driven cavity problem causes recirculation phenomenon because of the nonzero boundary condition of the velocity on the top

¹ Depto. Matemáticas, UAM-I; 09340 México D:F., México. E-mail: anc@xanum.uam.mx

² F. C.C., Benemérita Universidad Autónoma de Puebla; Puebla, Pue., México. E-mail: bbj@solarium.cs.buap.mx

wall which together with buoyancy from the vertical temperature gradient makes the problem more difficult to deal with. Moreover, since the isothermal case it is known that the variation of the aspect ratio A makes the flow more unstable, Nicolás and Bermúdez (2005) and Bruneau and Jouron (1990).

Mixed convection results are scarce Iwatsu, Hyun and Kuwahara (1993), Bermúdez and Nicolás (1999), and even more with velocity-vorticity variables, Fusegi and Farouk (1986) and Arafmanesh, Nahafi and Abdi (2008). Moreover, to solve the system of equations in these variables is more difficult, at least with a numerical procedure similar to the one applied for solving an analogous non-linear elliptic system that results after time discretization with the stream function-vorticity formulation, Nicolás and Bermúdez (2005). The mixed convection flows has engineering applications like those for design of interchange of heat, Iwatsu, Hyun and Kuwahara (1993).

Based on the fact that heat transfer is of interest as well, the results are complemented with the local $N(x)$ and global \overline{Nu} Nusselt numbers. Moreover, to support the results are correct mesh size and time-step independence studies are carried out.

2 Mathematical model and numerical method

Let $\Omega \subset R^N (N = 2, 3)$ be the region of the flow of an unsteady thermal viscous incompressible fluid in a gravitational system, and Γ its boundary. This kind of flows is governed by the non-dimensional system, in $\Omega \times (0, T), T > 0$,

$$\begin{cases} \mathbf{u}_t - \frac{1}{Re} \nabla^2 \mathbf{u} + \nabla p + \mathbf{u} \nabla \mathbf{u} = \mathbf{f} & (a) \\ \nabla \cdot \mathbf{u} = 0 & (b) \\ \theta_t - \frac{1}{RePr} \nabla^2 \theta + \mathbf{u} \cdot \nabla \theta = 0, & (c) \end{cases} \quad (1)$$

known as the Boussinesq approximation in primitive variables, velocity \mathbf{u} and pressure p , if $\mathbf{f} = \frac{Gr}{Re^2} \theta \mathbf{e}$, where θ is the dimensionless temperature of the flow, and \mathbf{e} is the unit vector in the gravity direction \mathbf{g} . The dimensionless parameters Re , Gr and Pr are the Reynolds, Grashof and Prandtl numbers. These parameters are given by $Re = UL/\nu$, with $\nu = \frac{UL}{Re}$ =kinematic viscosity, $Pr = \kappa/\mu c_p$; g is the gravitational constant L and U are the length and the velocity of reference. The thermal coefficients, μ =dynamic viscosity and c_p =the specific heat are also involved.

The system must be supplemented with appropriated initial and boundary conditions. For instance $\mathbf{u}(\mathbf{x}, 0) = \mathbf{u}_0(\mathbf{x})$ ($\nabla \cdot \mathbf{u}_0 = 0$) and $\theta(\mathbf{x}, 0) = \theta_0(\mathbf{x})$ in Ω ; $\mathbf{u} = \mathbf{g}$ ($\int_{\Gamma} \mathbf{g} \cdot \mathbf{n} d\Gamma = 0$) and $B\theta = 0$ on $\Gamma, t \geq 0$, where B is a temperature boundary operator which can involve Dirichlet, Neumann or mixed boundary conditions.

Taking the curl in (1a), one obtains the non-dimensional form of the vorticity ω transport equation, in $\Omega \times (0, T)$, given by

$$\omega_t - \frac{1}{Re} \nabla^2 \omega + \mathbf{u} \cdot \nabla \omega = \omega \cdot \nabla \mathbf{u} + \mathbf{f}, \quad (2)$$

where the new \mathbf{f} is the curl of the old one and the vorticity vector ω is given by

$$\omega = \nabla \times \mathbf{u} \quad (3)$$

Then, (2) says that vorticity is diffused, convected, and stretched, Chorin and Marsden (2000). Taking the curl in (3), using the identity $\nabla \times \nabla \times \mathbf{a} = -\nabla^2 \mathbf{a} + \nabla(\nabla \cdot \mathbf{a})$ and (1b), we get the following velocity Poisson equation

$$\nabla^2 \mathbf{u} = -\nabla \times \omega \quad (4)$$

Hence, equations (2), with the corresponding \mathbf{f} depending on θ , and (4), both coupled to (1c), give the Boussinesq approximation in velocity-vorticity variables. It can be easily verified that the vorticity, scalar, ω transport equation, in $\Omega \times (0, T)$, $\Omega \subset R^2$, is given by

$$\omega_t - \frac{1}{Re} \nabla^2 \omega + \mathbf{u} \cdot \nabla \omega = \frac{Gr}{Re^2} \frac{\partial \theta}{\partial x}; \quad (5)$$

moreover, from the 2D restriction in (3),

$$\omega = \frac{\partial u_2}{\partial x} - \frac{\partial u_1}{\partial y} \quad (6)$$

and, from (4), two Poisson equations for the velocity components are obtained

$$\begin{cases} \nabla^2 u_1 = -\frac{\partial \omega}{\partial y} & (a) \\ \nabla^2 u_2 = \frac{\partial \omega}{\partial x} & (b) \end{cases} \quad (7)$$

Then, the vector Boussinesq approximation system (2) and (4) coupled to (1c) is reduced to a scalar system of four equations in 2D: one given by (5) and two for u_1 and u_2 given by (7), coupled to (1c); (5) and (7) are related through (6) from which the boundary condition for ω in (5) should be obtained from that of $\mathbf{u} = (u_1, u_2)$.

To approximate the time derivatives that appear in the vorticity and temperature equations (5) and (1c), the following well known second-order approximation is applied

$$f_t(\mathbf{x}, (n+1)\Delta t) = \frac{3f^{n+1} - 4f^n + f^{n-1}}{2\Delta t}, \quad (8)$$

where $\mathbf{x} \in \Omega$, $n \geq 1$, Δt denotes the time step, and $f^r \equiv f(\mathbf{x}, r\Delta t)$, assuming f is smooth enough.

Then, from (5), (7), and (1c), a fully implicit time-discretization gives a nonlinear system of elliptic equations, at each time level $(n + 1)\Delta t$, which reads

$$\left\{ \begin{array}{l} \nabla^2 u_1^{n+1} = -\frac{\partial \omega^{n+1}}{\partial y} \\ \nabla^2 u_2^{n+1} = \frac{\partial \omega^{n+1}}{\partial x}, \quad \mathbf{u}^{n+1}|_{\Gamma} = \mathbf{u}_{bc} \\ \alpha \omega^{n+1} - \nu \nabla^2 \omega^{n+1} + \mathbf{u}^{n+1} \cdot \nabla \omega^{n+1} = \frac{Gr}{Re^2} \left(\frac{\partial \theta}{\partial x}\right)^{n+1} + f_{\omega}, \quad \omega^{n+1} = \omega_{bc} \\ \alpha \theta^{n+1} - \gamma \nabla^2 \theta^{n+1} + \mathbf{u}^{n+1} \cdot \nabla \theta^{n+1} = f_{\theta}, \quad B\theta^{n+1}|_{\Gamma} = 0, \end{array} \right. \quad (9)$$

where $\alpha = \frac{3}{2\Delta t}$, $f_{\omega} = \frac{4\omega^n - \omega^{n-1}}{2\Delta t}$, $f_{\theta} = \frac{4\theta^n - \theta^{n-1}}{2\Delta t}$, $\gamma = \frac{1}{PrRe}$, and $\frac{UL}{Re}$ has been replaced by the kinematic viscosity coefficient ν ; \mathbf{u}_{bc} and ω_{bc} denote the boundary condition for \mathbf{u} and ω , and B the temperature boundary operator. To initiate (9), $(u_1^1, u_2^1, \omega^1, \theta^1)$ need to be computed: a first order approximation may be applied on a subsequence with smaller time step; a system of the form (9) is also obtained. Once $\{u_1, u_2, \omega, \theta\} = \{u_1^{n+1}, u_2^{n+1}, \omega^{n+1}, \theta^{n+1}\}$ is replaced, at time level $(n + 1)\Delta t$, a fixed point iterative process may be used to solve system (9), which can be seen either as an adaptation of the one for mixed convection in stream function-vorticity variables, Nicolás and Bermúdez (2005), or as an extension to mixed convection of the one for isothermal flows in velocity-vorticity variables, Nicolás and Bermúdez (2007).

If we denote

$$\begin{aligned} R_{\omega}(\omega, \mathbf{u}) &\equiv \alpha \omega - \nu \nabla^2 \omega + \mathbf{u} \cdot \nabla \omega - \frac{Gr}{Re^2} \frac{\partial \theta}{\partial x} - f_{\omega} \quad \text{in } \Omega \\ R_{\theta}(\theta, \mathbf{u}) &\equiv \alpha \theta - \gamma \nabla^2 \theta + \mathbf{u} \cdot \nabla \theta - f_{\theta} \quad \text{in } \Omega, \end{aligned}$$

system (9) is equivalent, in Ω , to

$$\left\{ \begin{array}{l} \nabla^2 u_1 = -\frac{\partial \omega}{\partial y} \\ \nabla^2 u_2 = \frac{\partial \omega}{\partial x}, \quad \mathbf{u}|_{\Gamma} = \mathbf{u}_{bc} \\ R_{\theta}(\theta, \mathbf{u}) = 0, \quad B\theta|_{\Gamma} = 0 \\ R_{\omega}(\omega, \mathbf{u}, \theta) = 0, \quad \omega|_{\Gamma} = \omega_{bc}. \end{array} \right. \quad (10)$$

Then, (10) is solved by the fixed point iterative process:

With $\omega^0 = \omega^n$ and $\theta^0 = \theta^n$ given, solve until convergence on θ and ω , in Ω ,

$$\left\{ \begin{array}{l} \nabla^2 u_1^{m+1} = -\frac{\partial \omega^m}{\partial y} \\ \nabla^2 u_2^{m+1} = \frac{\partial \omega^m}{\partial x}, \quad \mathbf{u}^{m+1}|_{\Gamma} = \mathbf{u}_{bc} \\ \theta^{m+1} = \theta^m - \rho_{\theta}(\alpha I - \gamma \nabla^2)^{-1} R_{\theta}(\theta^m, \mathbf{u}^{m+1}), \quad B\theta^{m+1}|_{\Gamma} = 0, \quad \rho_{\theta} > 0, \\ \omega^{m+1} = \omega^m - \rho_{\omega}(\alpha I - \nu \nabla^2)^{-1} R_{\omega}(\omega^m, \mathbf{u}^{m+1}, \theta^{m+1}), \quad \omega^{m+1}|_{\Gamma} = \omega_{bc}^m, \quad \rho_{\omega} > 0, \end{array} \right. \quad (11)$$

then take $(u_1^{n+1}, u_2^{n+1}, \theta^{n+1}, \omega^{n+1}) = (u_1^{m+1}, u_2^{m+1}, \theta^{m+1}, \omega^{m+1})$.

Finally, system (11) is equivalent, in Ω , to

$$\left\{ \begin{array}{l} \nabla^2 u_1^{m+1} = -\frac{\partial \omega^m}{\partial y} \\ \nabla^2 u_2^{m+1} = \frac{\partial \omega^m}{\partial x}, \quad \mathbf{u}_{bc}^{m+1}|_{\Gamma} = \mathbf{u}_{bc} \\ (\alpha I - \beta \nabla^2)\theta^{m+1} = (\alpha I - \gamma \nabla^2)\theta^m - \rho_{\theta} R_{\theta}(\theta^m, \mathbf{u}^{m+1}), \quad \rho_{\theta} > 0, \quad B\theta^{m+1}|_{\Gamma} = 0 \\ (\alpha I - \nu \nabla^2)\omega^{m+1} = (\alpha I - \nu \nabla^2)\omega^m - \rho_{\omega} R_{\omega}(\omega^m, \mathbf{u}^{m+1}, \theta^{m+1}), \quad \rho_{\omega} > 0, \\ \omega^{m+1}|_{\Gamma} = \omega_{bc}^m. \end{array} \right. \quad (12)$$

It turns out that at each iteration *four* uncoupled, symmetric linear elliptic problems associated with the operators $\alpha I - \gamma \nabla^2$ and $\alpha I - \nu \nabla^2$, and two with ∇^2 have to be solved; it should be noted that the non-symmetric part for θ and ω has been taken into the right hand side thanks to the iterative process.

It is well known that for the space discretization of elliptic problems either finite differences or finite elements may be used as far as rectangular domains are concerned; it is also known that in either case efficient solvers exist. For the finite element case, variational formulations have to be chosen and then restrict them to finite dimensional spaces, like those in Glowinski (2003) and Gunzburger (1989). For the specific results in the next section, the second order finite difference approximation of the Fishpack solver in rectangular domains, Adams, Scharztrauber and Sweet (1980), is used. Then, such second order approximation in space combined with the second order approximation in (8) for the first derivatives in time, the approximation with second order central differences at the interior points, and with (8) on the boundary, for all the first derivatives of ω and θ , appearing in (11), those for the Neumann type boundary condition for θ appearing in the next section, including those that appear in the local Nusselt number $Nu(x)$, and the second order trapezoidal rule (in all the interval) to calculate the global Nusselt number $\bar{N}u$, imply that the whole discrete problem relies on second order discretizations only.

3 Numerical experiments

The numerical experiments take place in rectangular domains $\Omega = (0, a) \times (0, b)$, $a, b > 0$, in connection with the lid-driven cavity problem; then, the boundary condition of \mathbf{u} is given by $\mathbf{u} = (1, 0)$ at the moving boundary $y = b$ and $\mathbf{u} = (0, 0)$ elsewhere. On the other hand, the boundary condition for the temperature (given implicitly on the operator B in (12)) is given by

$$\begin{cases} \frac{\partial \theta}{\partial n} = 0 \text{ on } \Gamma|_{x=0,a}; \\ \theta = \theta_0 \equiv 0 \text{ on } \Gamma|_{y=0}, \theta = \theta_1 \equiv 1 \text{ on } \Gamma|_{y=b}, \end{cases}$$

which means that the top wall, $(x, y) = (x, b)$, is maintained at a higher temperature than the bottom wall, $(x, y) = (x, 0)$, and the lateral walls, $(x, y) = (0, y)$ and $(x, y) = (a, y)$, are insulated. Then, the fluid motion is caused by buoyancy from the vertical temperature gradient and by the nonzero velocity on the top wall.

The local Nusselt number Nu measures the heat transfer at each point on the hot wall into the fluid, where the temperature is specified, and the global Nusselt number \overline{Nu} measures the average of the heat transfer on the wall. These non-dimensional parameters, on the hot wall under study, are defined by

local Nusselt number:

$$Nu(x) = \frac{\partial \theta}{\partial y} \Big|_{y=b}$$

global Nusselt number:

$$\overline{Nu} \Big|_{y=b} = \frac{1}{A} \int_0^a Nu(x) dx,$$

with $A = \frac{b}{a}$. It is assumed that the cavity is filled with air, then the Prandtl number Pr is set to $Pr = 0.72$; then, from hereafter the flows will be depending on Re , Gr , and A only. We consider $100 \leq Gr \leq 100000$, $400 \leq Re \leq 1000$, and $0 < A \leq 3$. The flows depart from rest, then the initial condition for \mathbf{u} and θ are $\mathbf{u}(\mathbf{x}, 0) = \mathbf{0}$ and $\theta(\mathbf{x}, 0) = 0$. The mesh sizes are denoted by h_x , h_y and the time step by Δt ; they will be specified for each case under study. The results correspond to flows at steady state and are reported through the streamlines and the isotherms, and they are complemented with their heat transfer through $Nu(x)$ and \overline{Nu} .

To justify the flows that follow are correct, a mesh size and time-step independence studies are made in terms of the point-wise discrete L_∞ relative error on the closure of the cavity $\overline{\Omega}$, Nicolás and Bermúdez (2005),

$$\begin{cases} \Delta t \text{ fixed : } & \frac{\|f_{hx1,hy1;\Delta t} - f_{hx2,hy2;\Delta t}\|_\infty}{\|f_{hx1,hy1;\Delta t}\|_\infty}, \\ \{h_x, h_y\} \text{ fixed : } & \frac{\|f_{hx,hy;\Delta t1} - f_{hx,hy;\Delta t2}\|_\infty}{\|f_{hx,hy;\Delta t1}\|_\infty} \end{cases}$$

In connection with this, for $Re = 400$, $Gr = 100$, and $A = 2$ a mesh size inde-

pendence study was performed considering the uniform meshes, until the boundary: 1) $(h_x, h_y) = (\frac{1}{64}, \frac{2}{128})$, 2) $(h_x, h_y) = (\frac{1}{128}, \frac{2}{256})$, 3), $(h_x, h_y) = (\frac{1}{256}, \frac{2}{512})$, and $(h_x, h_y) = (\frac{1}{384}, \frac{2}{768})$; using $\Delta t = 0.001$ fixed. On this regard, Table 1 shows the corresponding discrepancies for the stream function ψ and the temperature θ . Then, from this Table the correct flow is obtained with the mesh in 2). Concerning the time-step independence study, with $(h_x, h_y) = (\frac{1}{128}, \frac{2}{256})$ fixed, a calculation was made with smaller and bigger time-steps: $\Delta t = 0.0001$ ($\Delta t3$), $\Delta t = 0.01$ ($\Delta t1$), and $\Delta t = 0.001$ ($\Delta t2$). Table 2 shows the discrepancies for ψ and θ . From this Table we see that $\Delta t2 = 0.001$ is enough to get the right flows. The description of the results follows.

Table 1: Mesh independence study

Mesh	ψ	θ
1 vs 2	0.3211	0.1428
1 vs 3	0.3087	0.1286
1 vs 4	0.2999	0.1241
2 vs 3	0.0393	0.0145
2 vs 4	0.0577	0.0192
3 vs 4	0.0177	0.0047

Table 2: Time-step independence study

Time	ψ	θ
$\Delta t1$ vs $\Delta t2$	0.0015	0.00028
$\Delta t1$ vs $\Delta t3$	0.0019	0.00047
$\Delta t2$ vs $\Delta t3$	0.00041	0.00047

For $Re = 400$ and $Gr = 100$, Figures 1, 2, 3, 4, and 5 show successively the flows with $A = 1, 2, \frac{1}{2}, 3,$ and $\frac{1}{3}$: streamlines (left or up) and isotherms (right or down); the respective meshes are $h_x = h_y = \frac{1}{128}$; $h_x = \frac{1}{128}, h_y = \frac{2}{256}$; $h_x = \frac{1}{256}, h_y = \frac{3}{768}$; and $h_x = \frac{3}{384}, h_y = \frac{1}{128}$. In these cases we do not know other results to compare with but they are reasonable since the deformation of streamlines and isotherms is similar to the ones expected from $A = 1$ in Figure 1; moreover, they must be correct from the mesh size and time-step independence studies.

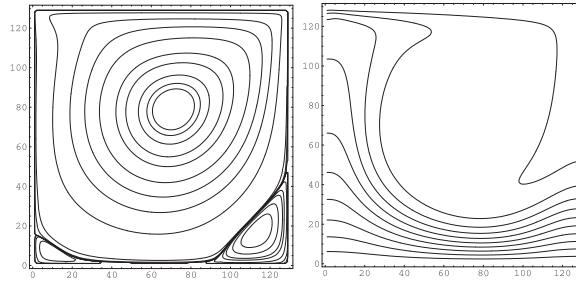
For $Re = 1000$ and $Gr = 100$, Figures 6, 7 and 8 picture successively the flows with $A = 1, A = 2,$ and $A = \frac{1}{2}$ with meshes $h_x = h_y = \frac{1}{128}$; $h_x = \frac{1}{128}, h_y = \frac{2}{256}$; and

Table 3: Ψ_{max} , Ψ_{min} and \bar{Nu} : $Re = 400$, $Gr = 100$; $h = 1/128$

A	Ψ_{max}	Ψ_{min}	\bar{Nu}
3	0.010	-0.122	1.185
2	0.010	-0.122	1.215
1	8.011E-04	-0.122	3.654
1/2	0.017	-0.187	5.77
1/3	0.02	-0.199	7.173

Table 4: Ψ_{max} , Ψ_{min} and \bar{Nu} : $Re = 1000$, $Gr = 100000$; $h = 1/128$

A	Ψ_{max}	Ψ_{min}	\bar{Nu}
3	0.026	-0.126	3.083
2	0.023	-0.124	3.310
1	0.002	-0.12	7.206
1/2	0.07	-0.256	17.490
1/3	0.11	-0.258	22.385

Figure 1: $Re = 400$, $Gr = 100$, $A = 1$; streamlines (left), isotherms (right)

$h_x = \frac{2}{256}$, $h_y = \frac{1}{128}$. For $A = 1$, the result agrees very well with that reported in Iwatsu, Hyun and Kuwahara (1993), Bermúdez and Nicolás (1999), and Nicolás and Bermúdez (2005).

For $Re = 1000$ and $Gr = 100000$, Figures 9, 10 and 11 display successively the flows with $A = 1$, $A = 2$, and $A = \frac{1}{2}$ with meshes $h_x = h_y = \frac{1}{128}$; $h_x = \frac{1}{128}$, $h_y = \frac{2}{256}$; and $h_x = \frac{2}{256}$, $h_y = \frac{1}{128}$.

In connection with the heat transfer through $Nu(x)$ in the upper wall $(x,y)=(x,1)$; depending on A , x varies on $0 \leq x \leq 3$ for $A = \frac{1}{3}$, $0 \leq x \leq 2$ for $A = \frac{1}{2}$, and $0 \leq x \leq 1$ for $A = 1, 2, 3$. Then, with $A = \frac{1}{3}, \frac{1}{2}, 1, 2$, and 3 : Figure 12 displays the heat transfer $Nu(x)$ for $Re = 400$ and $Gr = 100$, the graphs for $A = 2$ and $A = 3$ are overlapped; the picture shows that the heat transfer increases as A decreases, we also observe that the maximum value of $Nu(x)$ occurs near $x = 0$, while the minimum occurs in $x=1$ for $A = 1, 2, 3$, in $x = 2$ for $A = \frac{1}{2}$, and in $x = 3$ for $A = \frac{1}{3}$. Figure 13, shows

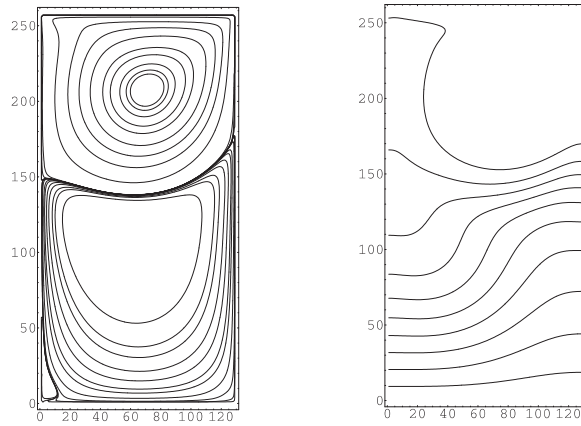


Figure 2: $Re = 400$, $Gr = 100$, $A = 2$; streamlines (left), isotherms (right)

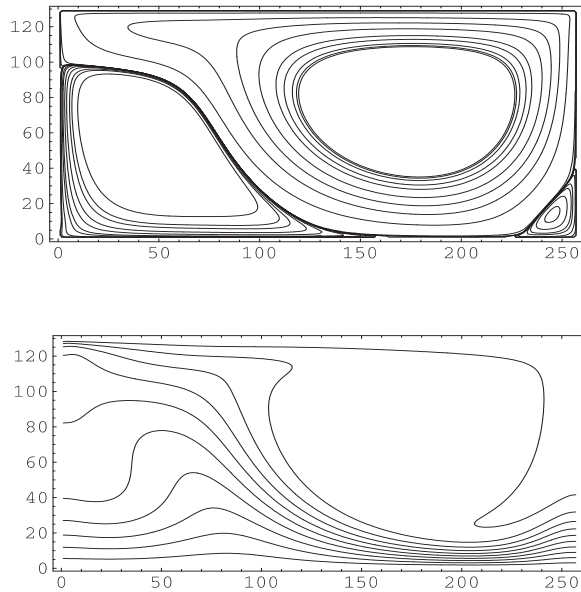


Figure 3: $Re = 400$, $Gr = 100$, $A = 1/2$; streamlines (up), isotherms (down)

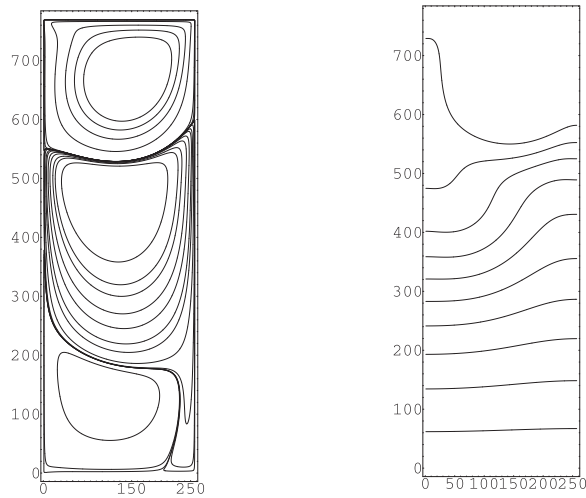


Figure 4: $Re = 400$, $Gr = 100$, $A = 3$; streamlines (left), isotherms (right)

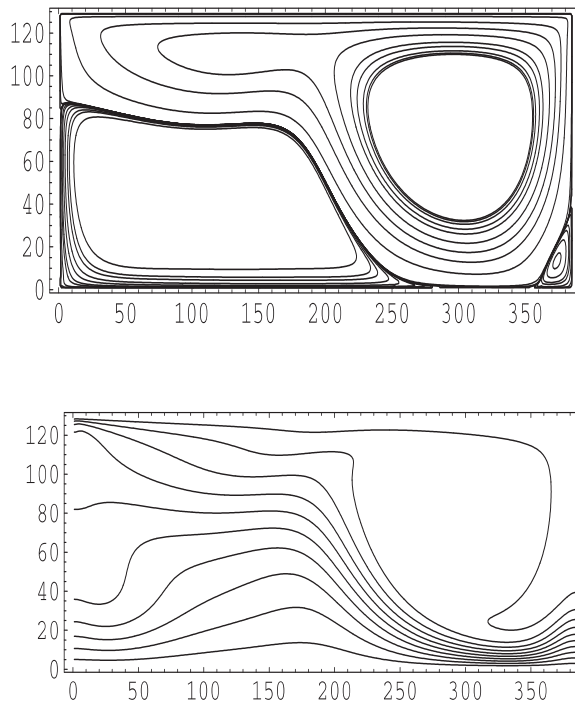


Figure 5: $Re = 400$, $Gr = 100$, $A = 1/3$; streamlines (up), isotherms (down)

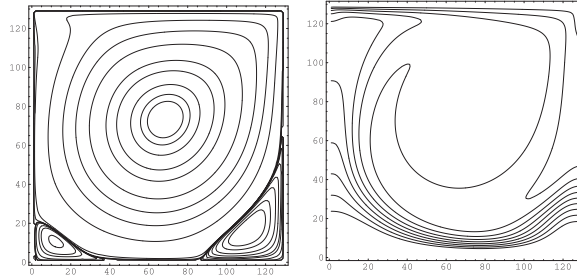


Figure 6: $Re = 1000, Gr = 100, A = 1$; streamlines (left), isotherms (right)

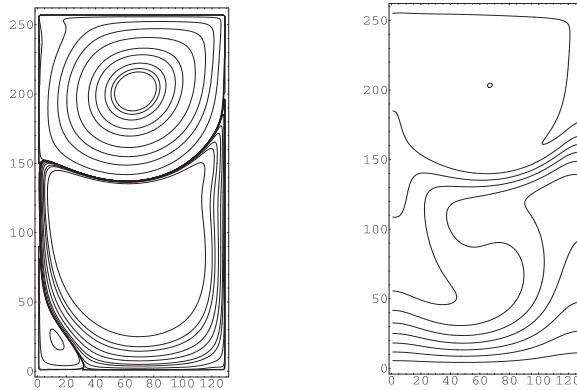


Figure 7: $Re = 1000, Gr = 100, A = 2$; streamlines (left), isotherms (right)

the heat transfer $Nu(x)$ for $Re = 1000$ and $Gr = 100000$. The graphs for $A = 2$ and $A = 3$ are almost overlapped. The heat transfer also increases, at a higher rate than the case before, as A decreases. We observe that the maximum value of $Nu(x)$ occurs near $x = 0$, while the minimum occurs in $x=1$ for $A = 1, 2,$ and 3 ; in $x = 2$ for $A = \frac{1}{2}$ and in $x = 3$ for $A = \frac{1}{3}$. In this case is notorious the appearance of one local minimum and maximum for $A = \frac{1}{2}$ and $\frac{1}{3}$. Some discussion follows in terms of Tables 3 and 4.

From Tables 3 and 4 follow that the fluid motion is very weak but it does not decrease as A increases for vertical cavities and it increases when A decreases for horizontal cavities; however, for vertical cavities there are more cells and the number of cells increases as A increases: the top one moving clockwise, the second one downwards counterclockwise, and so on. It is observed that the heat transfer, through $Nu(x)$, in Figures 12 and 13, and \overline{Nu} , is stronger, and: $Nu(x)$ increases as A decreases and \overline{Nu} decreases as A increases for vertical cavities and it increases as A decreases for horizontal cavities; that \overline{Nu} increases as A decreases can be strongly

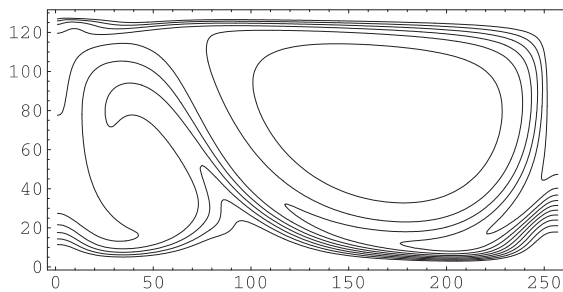
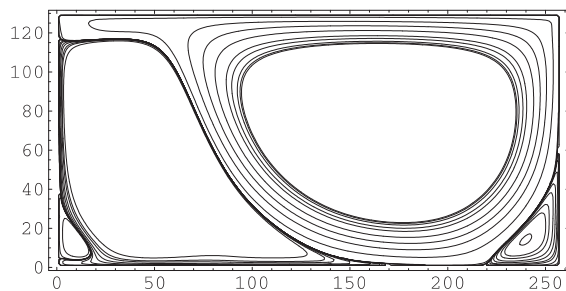


Figure 8: $Re = 1000$, $Gr = 100$, $A = 1/2$; streamlines (up), isotherms (down)

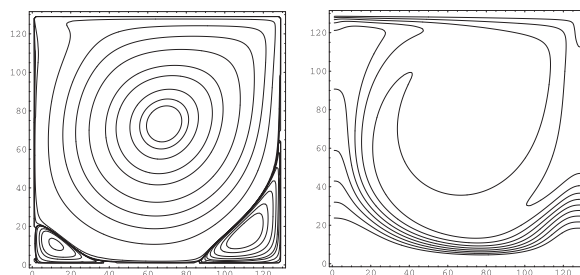


Figure 9: $Re = 1000$, $Gr = 100000$, $A = 1$; streamlines (left), isotherms (right)

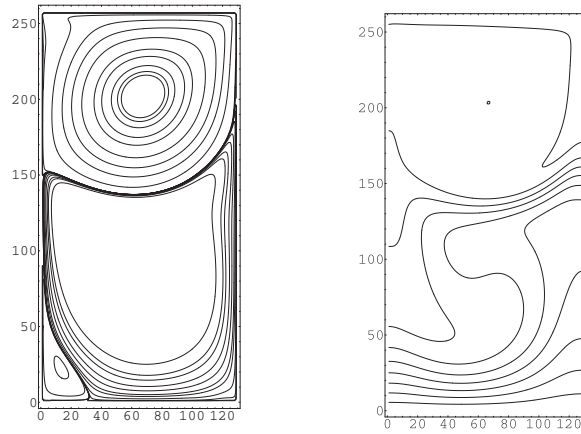


Figure 10: $Re = 1000$, $Gr = 100000$, $A = 2$; streamlines (left), isotherms (right)

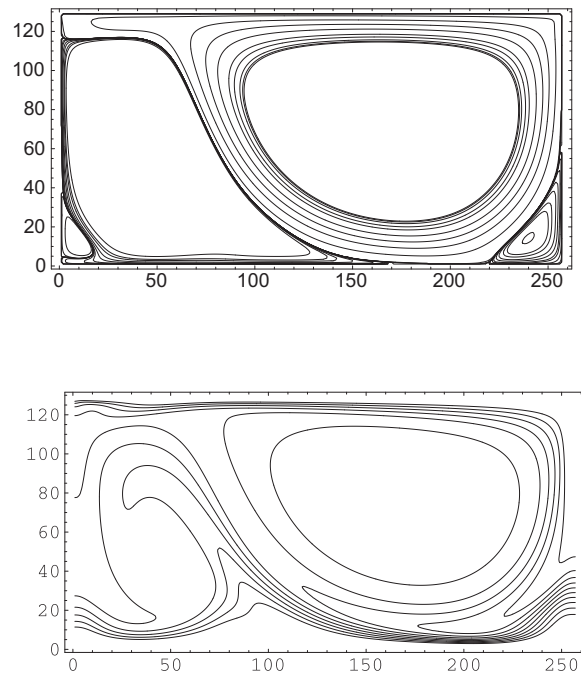


Figure 11: $Re = 1000$, $Gr = 100000$, $A = 1/2$; streamlines (up), isotherms (down)

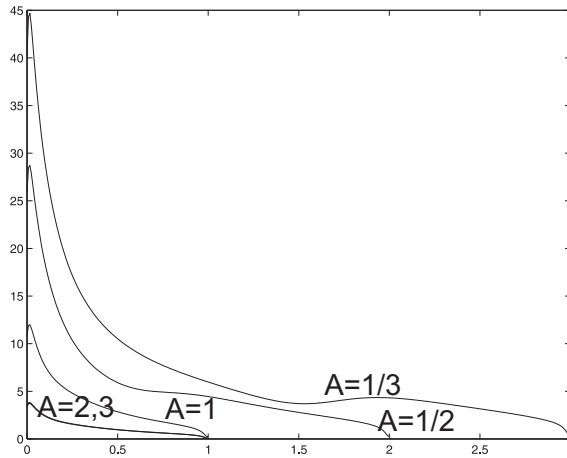


Figure 12: $Re=400$ and $Gr=100$: local Nusselt numbers for $A = 1, 2, 3, \frac{1}{2}$, and $\frac{1}{3}$

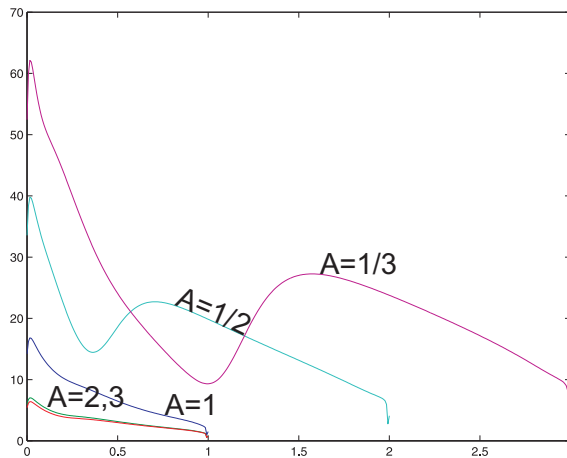


Figure 13: $Re=1000$, $Gr=100000$: local Nusselt numbers for $A = 1, 2, 3, \frac{1}{2}$ and $\frac{1}{3}$

associated to the increasing of the interval length of the hot wall where the heat transfer comes from, something like this happens with $Nu(x)$.

We would like to remark that for $Re = 1000$ with $Gr = 100$ and 100000 ; as it can be observed in Figures 6, 7, 8, and 9, 10, 11; the flows look very similar. The same happens with the local Nusselt numbers $Nu(x)$ and also with the corresponding properties that appear in Table 4. Because of this we do not present the Table for $Re = 1000$ and $Gr = 100$ neither its $Nu(x)$ graph.

4 Conclusions

We have been presented results on mixed convection flows in rectangular cavities using the unsteady Boussinesq approximation in velocity and vorticity variables. The results are obtained from the well known un-regularized driven cavity problem which since the isothermal case gives rise recirculation; moreover, on this regard it is known that the variation of the aspect ratio A makes the fluid flow more unstable. The results cover moderate values of the Reynolds number Re and the Grashof number Gr . The fluid motion is not stronger at all but it has some monotonic growth as A increases or decreases; however, for vertical cavities there is more motion activity, there are more cells and the number of cells increases as A increases: the top one moving clockwise, the second below counterclockwise, and so on. The heat transfer is stronger and it has also a monotonic growth as A increases or decreases; actually the heat transfer is stronger for horizontal cavities when A decreases, since the length of the hot wall increases. Preliminary results for higher values of the parameters show more activity on the fluid motion and on the heat transfer as well.

References

- Adams J., Schwarztrauber P. and Sweet R.**(1980): FISHPAK: A package of fortran subprograms for the solution of separable elliptic PDE's', newblock *The National Center for Atmospheric Research*, Boulder, Colorado, USA.
- Arefmanesh, A., M. Nahafi and H.Abdi.**(2008): Meshless local Petrov Galerkin Method with Unity Test Function for Non-Isothermal Fluid Flow. *CMES: Computer Modelling in Engineering and Sciences*: 25(1), 9-22.
- Bermúdez B. and Nicolás A.**,(1999): An Operator Splitting Numerical Scheme for Thermal/Isothermal Incompressible Viscous Flows. *Int. J. Num. Meth. Fluids*, 29, 397-410.
- Bruneau C. H., Jouron C.** (1990):An efficient scheme for solving steady incompressible Navier-Stokes equations, *J. of Computational Physics*, 89, 389-413.

Chorin A. J. and Marsden J. E.(2000)A Mathematical Introduction to Fluid Mechanics, Springer-Verlag, NY.

Fusegi T. and Farouk B. (1986): Predictions of Fluid Flow and Heat Transfer Problems by Vorticity-Velocity Formulation of the Navier-Stokes Equations. *J. of Computational Physics*, 65, 227-243.

Glowinski R.(2003):Hanbook of Numerical Analysis: Numerical Methods for Fluids (Part 3). *North-Holland Ed.*

Gunzburger M. D.(1989):Finite Element Methods for Viscous Incompressible Flows: A guide to theory, practice, and algorithms, *Academic Press, INC.*

Iwatsu, R.; Jae Min Hyun; and Kuwahara, K.(1993):Mixed convection in a driven cavity with a stable vertical temperature gradient. *Int. J. Heat and Mass Transf.*, 36, pp. 1601-1608.

Nicolás, A. and Bermúdez B.(2005):2D thermal/isothermal incompressible viscous flows. *Int. J. Numer. Meth. Fluids*, 48, pp. 349-366.

Nicolás, A. and Bermúdez B.(2007):2D Viscous incompressible flows by the velocity-vorticity Navier-Stokes equations. *CMES: Computer Modeling in Engineering and Sciences*, V. 20, N. 2, pp. 73-83.